Jagannath University Journal of Science
Volume 11, Number I, Jun. 2024, pp. 186–202
https://jnu.ac.bd/journal/portal/archives/science.jsp
ISSN 3005-4486 (Online), ISSN 2224-1698 (Print)

Heat Transfer and Entropy Generation on Free Convection Airflow inside a T-shaped Cavity Considering Inner Obstacles

Research Article

Bijan Krishna Saha[1,*], Md. Shafiul Alam[1], Nur Jahangir Moon[1] and Bishnu Pada Ghosh[2]

[1]*Department of Mathematics, University of Barishal, Barishal-8254, Bangladesh*
[2]*Department of Mathematics, Jagannath University, Dhaka-1100, Bangladesh*

DOI: https://doi.org/10.3329/jnujsci.v11i1.76702

Received: 15 May 2024, Accepted: 29 June 2024

ABSTRACT

In this study, a numerical analysis of heat and entropy generation on free convection of airflow is performed inside a T-shaped cavity with and without circular obstacles. The T-shaped cavity is formed with two symmetrically isothermal rectangular blocks. A cold temperature is maintained on the cavity's upper wall. The adiabatic walls are connected to heated wall at constant temperature. It is assumed that the flow is laminar, 2-D, and steadily incompressible. The finite element analysis is employed for solving the governing equations. The calculated results are compared and validated with the other published works. The dimensionless velocity (streamlines) and temperature (isotherms) are calculated and illustrated for varying Rayleigh numbers. It is found that the average Nusselt number at the heated walls and entropy generation inside the cavity increase with the increment of Rayleigh numbers. Moreover, the thermal performance effects on natural convection flow are investigated with circular obstacles inside the enclosure. Five cases without and with circular obstacles regarding the boundary conditions are investigated. It is found that the thermal performance of the cavity can be improved by adding two circular obstacles with cool boundary conditions. It is evident that the innovative structure by adding two circular obstacles with cool boundary conditions gives higher average Nusselt number and entropy generation whereas lower Bejan numbers for varying Rayleigh numbers. The study is performed for $Ra = 10^3 - 10^6$ and $Pr = 0.71$.

Keywords*: Free convection, Heat transfer, Isothermal blocks, T-shaped cavity, Computational fluid dynamics*

***Corresponding Author:** Bijan Krishna Saha
E-mail: bksaha@bu.ac.bd

Introduction

The enhancement of heat transfer through natural convection in a cavity's geometry has been the subject of extensive numerical and experimental research due to its significance and interest in engineering designs and related issues, including solar collectors, thermal insulation, electronic component cooling, and building design. Engineering system design and improvement greatly benefit from the analysis of heat transport and fluid dynamics. An infinite horizontal channel with an unlimited number of regularly spaced rectangular, heated, and isothermal bricks was numerically studied by (Amahmid et al. 1997). They investigated how the choice of computing domain affected the number of possible solutions. Every solution's impact on heat transfer and flow is investigated. Their studies reveal that even if the boundary requirements for this problem are symmetrical, the flow's symmetry is not always preserved. Through numerical analysis, (Momoniat et al. 2023) discovered that the characteristics of temperature gradients, streamlines, and heat flux within the square cavity were significantly impacted by the addition of extended surfaces.

A square cavity with a fin was taken into consideration by (Shi et al. 2003) in order to study laminar free conventional temperature transfer. In preparation for both current and upcoming enrollment, (Choi 1998) researched nanofluid technologies. (Yousaf and Usman 2015) examined the free convectional heat transfer in a square chamber with sinusoidal roughness. Because of the wide range of applications in the industry, researchers have focused a lot of attention on the influence of magneto-hydrodynamic free conventional temperature transmission in recent years. Using a nanofluid with a magnetic effect, (Sheikholeslami et al. 2014) investigated the impact of a sinusoidal external on free convectional temperature transport. According to the paper, the Hartmann number reduces the Nusselt number, while the volume and buoyancy force of nanoparticles show the opposite response. (Rahman et al. 2016) conducted the magnetic convection flow within the triangle cavity. After studying the effects of turbulent and laminar flows on natural convection, (Kuyper et al. 1993) came to the conclusion that there is a strong relationship between the Rayleigh number (Ra) and the Nusselt number (Nu). Additionally, (Sreedevi and Reddy 2021) conducted a numerical analysis of the heat transmission, flow, and entropy generation characteristics of a hybrid nanofluid consisting of aluminum oxide, carbon nanotubes, and ethylene glycol within a square cavity. The results showed that heat transport is reduced by the Hartmann number and increases with the Rayleigh number. (Islam et al. 2020) investigated the MHD convection temperature transformer inside the triangle chamber containing the nanofluid. The effect of the fin on the free convectional thermal flow inside the square chamber was presented by (Jani et al. 2011). They observed that, due to the increased buoyancy effect, the fin near the middle wall transmits heat more effectively. (Das et al. 2007) look at the technology and science of nanofluids.

Free convection heat transfer from vertical plates with horizontal rectangular grooves has been the subject of experimental and numerical research recently carried out by (Kwak and Song 2000). They investigated how Rayliegh's number affected each of the system's aspect ratios. In order to determine the heat transfer rate from each pitch for the specified geometries and Rayleigh numbers, they discovered forgiven conditions and secondary recirculation flows in the grooves and created a suitable link. (Desrayaud and Fichera 2002) investigated the natural convection in a vertical channel blocked by two adiabatic or isothermal ribs numerically in a different study. They discovered that the Rayleigh number's magnitude determines the ideal location for the ribs in terms of heat extraction.

In a more recent work, (Chaabane et al. 2022) conducted a numerical investigation to explore how buoyancy-driven flow is impacted by the irregular shape of a cavity. The chimney effect was investigated by (El Alami et al. 2004) using natural convection from a blocked vented cavity. They proved that: the average Nusselt number increases significantly with solid block height; the correlation found for the average Nusselt number is similar to that found in the case of blocked chimneys; and the appearance of recirculation cells is caused by the amplification of heat transfer by the increase in the Rayleigh number.

According to (Asad et al. 2019), a numerical analysis of spontaneous convective flow with magnetic impact was conducted. In order to determine the best nanofluid design for heat augmentation, Natural convection of nanofluids between a sinusoidal cylinder and a rectangular hollow was investigated by (Alhashash and Saleh 2023). The results showed that increasing the heat transfer rate with 1% alumina particles is possible. (Alhajaj et al. 2020) investigated the nanofluid flow properties in the channels. Greenhouse effects and Brownian motion of flow in channels using nanofluid were studied by (Saghir et al. 2021). (Alam et al. 2022) carried out an analysis of the buoyancy-driven convection transport with magnetic effect in the semi-circular cavity. A square wavy cavity with a single vertical fin fixed to its lower heated wall was the subject of a numerical simulation of free convection MHD heat transfer by (Fayz-Al-Asad et al. 2019). Some related works can be found in (Sheikholeslami et al. 2014, Shi et al. 2003, Sreedevi and Reddy 2021, Yousaf and Usman 2015).

The study emphasizes that a wide range of applications, including electronic, cooling, energy storage, solar thermal technologies, and nuclear reactor systems, can be made with enclosed cavities. Numerous cavity shapes, such as square, rectangular, triangle, trapezoidal, semicircular, hexagonal, U-shaped, and others, have been taken into consideration in this study. The flow and temperature behavior inside the cavities are influenced by various boundary conditions that are applied to the cavity walls. The analysis takes into account several thermal boundary conditions, including temperature, heat flux, adiabatic, and isothermal. This is one particular application of the T-shaped cavity. The cavities in the shape of teeth are made to fit together perfectly, making the most of the cold storage system's available area. This design includes elements intended to reduce heat transmission between objects kept in various compartments, maintaining a constant temperature inside the system and improving overall effectiveness. The design facilitates uniform cooling across the T-shaped cavities by encouraging improved air circulation within the storage system, hence further optimizing temperature management. The aim of this research paper is the following: (a) to increase thermal performance inside the cavity, (b) to understand the physical application of the enclosure, (c) to investigate thermal performance effects on natural convection of air inside a T-shaped cavity with and without obstacles for different thermal conditions. In this paper, we have first briefly discussed the free convective heat transfer and entropy generation of fluid dynamics. Then CAD modeling and numerical analysis are described precisely.

Physical Model

Figure 1 shows a schematic of the problem including the coordinate system and boundary conditions. It illustrates the shape of a T-shaped chamber with identical rectangular blocks set on the bottom wall, measuring h in height and L in width.

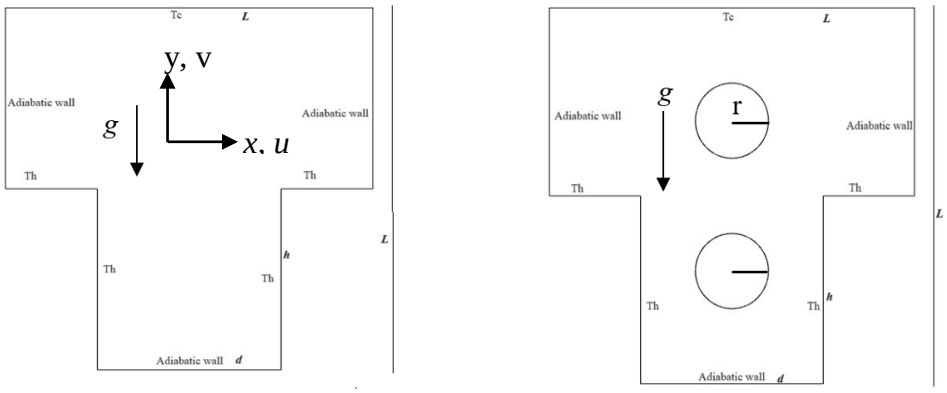

Fig. 1. Physical model without and with obstacles.

The blocks are set hot T_h and connected with the adiabatic surfaces. The upper wall is maintained at a cold temperature T_c. Here, we have also considered two circular obstacles inside the T-shaped cavity as shown in Figure 1. In a rectangular "T" shaped cavity, the flow is thought to be two-dimensional, incompressible, and laminar flow. The fluid under investigation is air, and all physical characteristics are taken to be constant at average temperature T_0 except density, which is permitted to vary with temperature in the buoyancy term. The dimensionless temperatures of hot and cold walls are set with -0.5 and 0.5 respectively. The circle obstacles are may be cold, hot and adiabatic. The dimensionless radius r of the circle is 0.05. Here, Rayleigh number is 10^3 and 10^6 and Prandtl number is 0.71 (air).

"T" shaped cavity in two dimensional coordinates:

Position	Coordinate	Width	Height
Upper rectangle	(0.0)	0.5	0.25
Lower rectangle	$(0.125, -0.25)$	0.25	0.5
Position	Radius (r)	X-coordinate	Y-coordinate
Upper circle	0.05	0.25	0.1
Lower circle	0.05	0.25	-0.1

Here, $x = h$ and $0 \leq y \leq d$; y= d and $0 \leq x \leq h$. The dimensionless velocity components are U and V which are 0. On the left and right edges of the computational domain, symmetry requirements have been applied. In a dimensionless setting, X and Y, or height (H) and breadth (D), are the pertinent boundary conditions. The hot temperature is 30^0C and cold temperature is 10^0C.

Mathematical Model

The governing equations are set according to the principles of conservation of mass. Momentum and energy for solving the "T"-shaped cavity model numerically. In the fluid domain within the T-shaped cavity, the equations regarding heat conduction at cold/hot walls are also considered in our simulation. For the mathematical formulation, we assume 2-D incompressible steady and laminar flow. The two-dimensional Navier–Stokes equations are presented in a dimensional format, as below (Saha et al. 2024):

$$\frac{\partial u}{\partial x} + \frac{\partial v}{\partial y} = 0 \qquad (1a)$$

$$\rho\left(u\frac{\partial u}{\partial x}+v\frac{\partial u}{\partial y}\right)=-\frac{\partial p}{\partial x}+\mu\left(\frac{\partial^2 u}{\partial x^2}+\frac{\partial^2 u}{\partial y^2}\right) \quad (1b)$$

$$\rho\left(u\frac{\partial v}{\partial x}+v\frac{\partial v}{\partial y}\right)=-\frac{\partial p}{\partial y}+\mu\left(\frac{\partial^2 v}{\partial x^2}+\frac{\partial^2 v}{\partial y^2}\right)+\rho g\beta(T-T_0) \quad (1c)$$

$$\rho C_p\left(u\frac{\partial T}{\partial x}+v\frac{\partial T}{\partial y}\right)=\alpha\left(\frac{\partial^2 T}{\partial x^2}+\frac{\partial^2 T}{\partial y^2}\right) \quad (1d)$$

The above set of equations (1a-1d) are reduced to dimensionless form together with the accompanying boundary conditions as follows:

$$X=\frac{x}{L},\ Y=\frac{x}{L},U=\frac{u}{\alpha L},V=\frac{v}{\alpha L},\theta=\frac{(T_f-T_c)}{(T_h-T_c)} \quad (2)$$

The stream function and vorticity are set as dimensionless in the following manner,

$$U=\frac{\partial\psi}{\partial Y},V=-\frac{\partial\psi}{\partial X}\ and\ \frac{\partial V}{\partial X}-\frac{\partial U}{\partial Y}=\Omega \quad (3)$$

The continuity equation satisfies the above-mentioned stream function equation. Simultaneously, the vorticity equation is calculated using the method of vorticity stream function, which eliminates the pressure term in the momentum equation. Hence, the dimensionless governing equations are presented below:

$$\frac{\partial^2\psi}{\partial X^2}+\frac{\partial^2\psi}{\partial Y^2}=-\Omega \quad (4a)$$

$$U\frac{\partial\Omega}{\partial X}+V\frac{\partial\Omega}{\partial Y}=Pr\left(\frac{\partial^2\Omega}{\partial X^2}+\frac{\partial^2\Omega}{\partial Y^2}\right)+RaPr\frac{\partial\theta}{\partial X} \quad (4b)$$

$$\left(U\frac{\partial\theta}{\partial X}+V\frac{\partial\theta}{\partial Y}\right)=\left(\frac{\partial^2\theta}{\partial X^2}+\frac{\partial^2\theta}{\partial Y^2}\right) \quad (4c)$$

Where *U, V, θ, X, Y* represent non-dimensional variables.

The quantities including *Ra* and *Pr* are defined as

$$Ra=\frac{g\beta(T_h-T_c)L^3}{\vartheta\alpha},Pr=\frac{\mu}{\rho\alpha} \quad (5)$$

The convective heat transfer and Nusselt number depend on the temperature gradient at a surface, $(\frac{\partial\theta}{\partial n})$, where n is a normal direction to the surface. The study evaluates the impact of thermal performance inside a "T" shaped cavity with and without obstacles.

The average Nusselt-Number is calculated by the following form:

$$Nu_{avg}=[\frac{1}{S}\int_0^S(-\frac{\partial\theta}{\partial X}|_{heated\ wall(Y)})dY+\frac{1}{S}\int_0^S(-\frac{\partial\theta}{\partial Y}|_{heated\ wall(X)})\,dX] \quad (6)$$

where S is the length of the heated wall.

Entropy Generation

A review of E_{gen} is conducted in order to assess the system's thermal efficiency. As a result, this study is consulted while evaluating the cavity's thermal performance. Our analysis revealed that the causes of E_{gen} were viscosity and thermal effects. The following is the dimensionless form of the local E_{gen}, local Be (Be_l), and total entropy (E_{total}) (Saha et al. 2024):

$$E_{total}=\left[\left(\frac{\partial\theta}{\partial x}\right)^2+\left(\frac{\partial\theta}{\partial y}\right)^2\right]+\varphi\left[2\left(\frac{\partial u}{\partial x}\right)^2+2\left(\frac{\partial v}{\partial y}\right)^2+\left(\frac{\partial u}{\partial y}+\frac{\partial v}{\partial x}\right)^2\right] \quad (7)$$

Here, the irreversibility factor is φ, which is equal to 10^{-4}.

The local Bejan number (Be_l) :

$$Be_l=\frac{\left(\frac{\partial\theta}{\partial x}\right)^2+\left(\frac{\partial\theta}{\partial y}\right)^2}{E_{total}} \quad (8a)$$

The average entropy generation (E_{avg}):

$$E_{avg} = \frac{\int\int E_{total}\ \mathrm{dx\ dy}}{\int\int\ \mathrm{dx\ dy}} \qquad (8b)$$

The average Bejan number (Be_{avg}):

$$Be_{avg} = \frac{\int_A\int_A Be_l\ \mathrm{dx\ dy}}{\int_A\int_A\ \mathrm{dx\ dy}} \qquad (8c)$$

Methodology and Validation

Numerical solutions of equations (1) to (5) were obtained by using a finite element method (FEM) based on Galerkin method. The governing equations subject to the boundary conditions are set for the present study. The model and simulation are solved by the COMSOL MULTIPHYSICS 6.1. For natural convection, we have discussed five cases (*Case-I:* T-shaped cavity without obstacle, *Case-II:* T-shaped cavity with two hot circular obstacles, *Case-III:* T-shaped cavity with two adiabatic circular obstacles, *Case-IV:* T-shaped cavity with upper hot and lower cool circular obstacles. *Case-V:* T-shaped with two cool circle obstacles) of models for $Ra = 10^3\ to\ 10^6$. A grid independence test was carried out by changing grid sizes and the findings are presented in Table 1. Following the data from Table 1, a grid size of 9128 was set to be optimal for the study. In the current investigation, the computational domain is divided into a set of non-overlapping regions called elements.

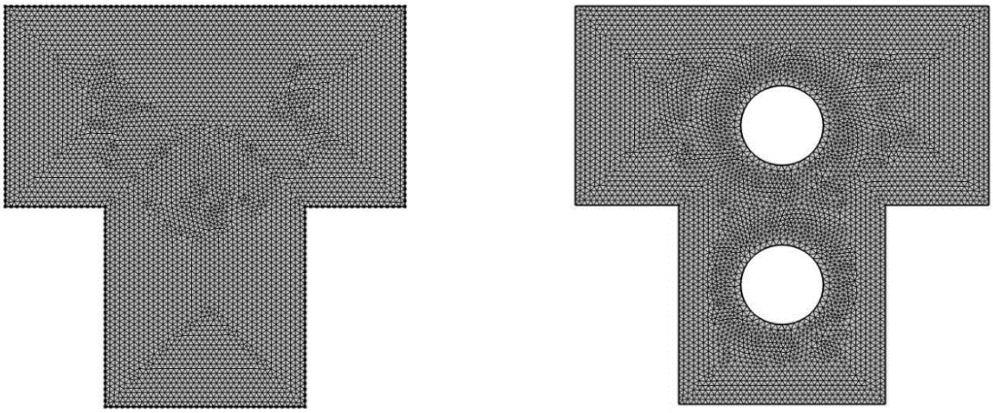

(a) T cavity without obstacle (b) T cavity with obstacles

Fig. 2. Schematic Presentation of the Grid without and with obstacles

Then the Galerkin weighted residual technique is used to convert the nonlinear governing partial differential equation into a system of integral equations that can be solved numerically (Hossain et al. 2023). The investigation involved in each term of these equations is performed by using Gauss quadrature method which leads to a set of non-linear algebraic equations. These equations are modified imposing boundary equations by Newton-Raphson iteration. Finally, these linear equations are solved by applying Triangular Factorization method. The "T" shaped cavity without obstacle and with circle obstacles are shown in Figure 2.

In order to validate the obtained numerical results, the contour of Entropy generation and Bejan number at values of $Ra = 10^3$ and $AR = 1$ within the square cavity are conducted as shown in Figure 3. The numerical results agree with the published work Ilis et al. (Ilis et al. 2008) which focused on square geometries. To increase the confidence of the present computational simulation, we have tested and compared with other published papers.

Table 1. Grid independence test for Nu_{avg}

Grid Size	Size of the Elements for T cavity without obstacle	Nu_{avg}	Size of the Elements for T cavity with obstacles	Nu_{avg}
GS-1	3068	5.4982	3558	9.4935
GS-2	7532	5.5823	8042	9.5813
GS-3	**9128**	**5.4967**	**9044**	**9.4967**
GS-4	18876	5.5575	22388	9.6268

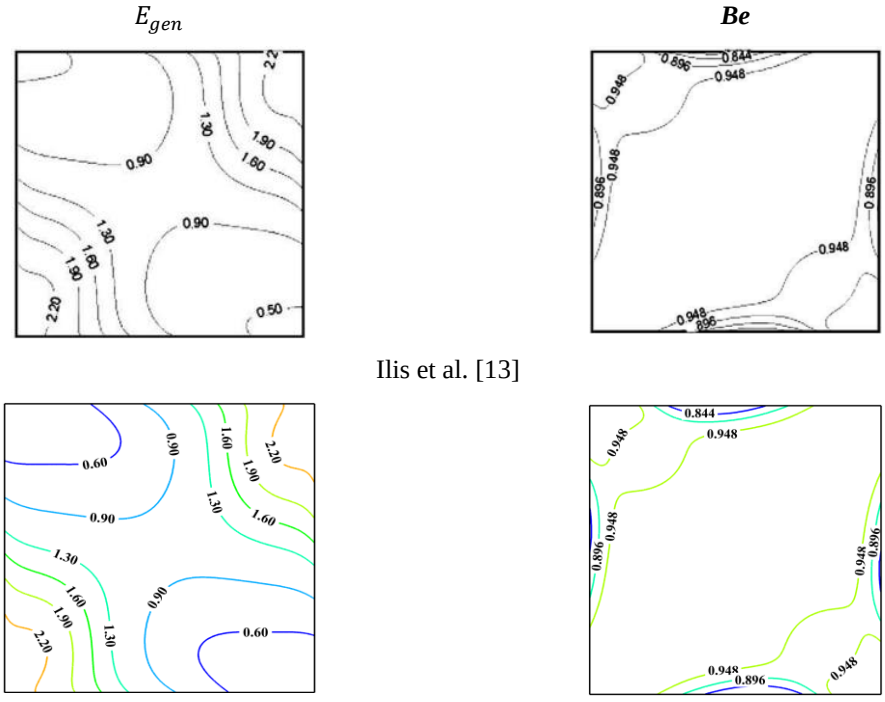

Fig. 3. Comparison between the published work vs present study for Entropy generation and Bejan contours at $Ra = 10^3$ and $AR = 1$ with $Pr = 0.71$

Result and discussion

In this work, finite element methods are implemented for solving the set of governing equations. This section aims to clarify the numerical solutions with graphical representation.

Streamlines and Isotherms

The findings for the T-shaped cavity with and without two round cylinders are shown and examined for a range of Rayleigh numbers ($Ra = 10^3 - 10^6$). In Figure 4 and Figure 5 illustrate the streamlines and isotherm contours for varying Rayleigh numbers in five cases.

Cases $Ra = 10^3$ $Ra = 10^4$ $Ra = 10^5$ $Ra = 10^6$

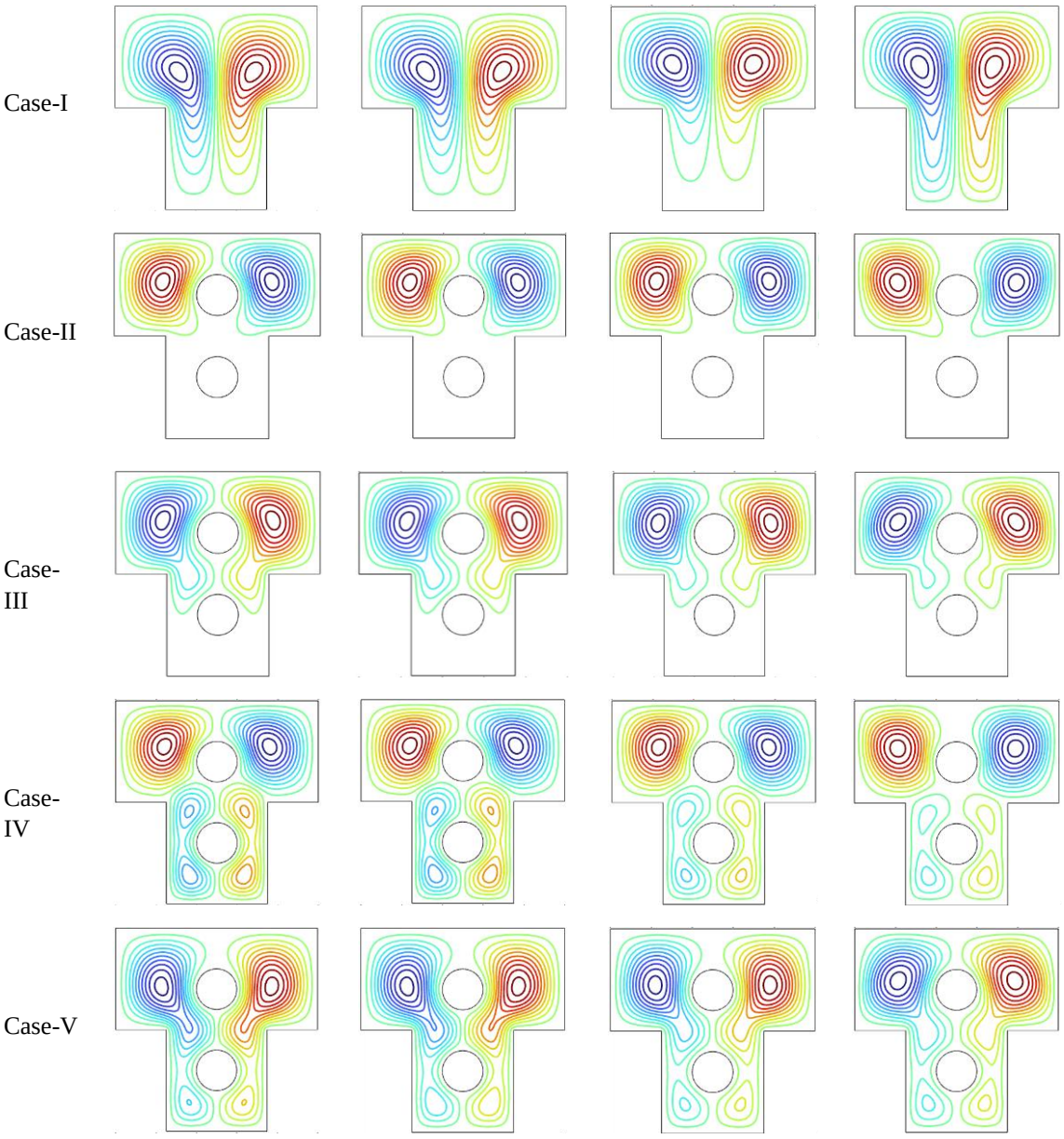

Fig. 4. Streamline contours for varying Rayleigh Number ($Ra = 10^3 - 10^6$)

The influence of thermal buoyancy forces on temperature and stream functions is expressed by varying Rayleigh numbers, which affect all contours. Actually, the isotherm and streamline contours depend on two parameters such as the boundary thermal conditions of two circular obstacles and varying Rayleigh numbers. In each case, the streamline contours are distributed symmetrically and smoothly into the whole cavity. In case-I, the streamline contours are symmetrically

smooth for increasing Rayleigh numbers (10^3 to 10^6). In case-III and case-V, when the Rayleigh number is increasing for the upper circular obstacle in adiabatic or cool, the streamlines are spread more smoothly than others.

In case-II and case-IV, when the Rayleigh number is decreasing and the upper circle obstacle is hot, the streamlines are spread more smoothly and created some vortices than others. In case-IV and case-V, streamline contours are represented by symmetrical rotating vortices that can be observed in the entire cavity. Rayleigh number (natural convection) causes variations in the shape of circulation. When the Rayleigh number (Ra) of the natural convection parameter is set to any value, the fluid in the cavity's left space rotates counterclockwise, while the air in the right-hand chamber rotates clockwise.

Circulating cells are developed to achieve higher values of buoyancy force ($Ra = 10^6$). This shows the hot air is accelerated more by the buoyancy effect. In each case, the isotherms are distributed smoothly in the whole "T" cavity when the Rayleigh number is increasing. We can control the thermal performance in the cavity by changing the thermal situation of obstacles and getting smooth isothermal curves. When the Rayleigh number is increasing from 10^3 to 10^6, the thermal buoyancy forces become strong.

In case-I, isotherm contours are found in parallel curves from top to bottom wall for $Ra = (10^3 - 10^5)$; the isotherm contours are twisted and distributed in the whole cavity for $Ra = 10^6$.

In case II, the isotherm contours are displayed as parallel curves from the top wall to the upper circle for $Ra = (10^3 - 10^5)$; the isotherm contours are twisted curves and distributed from the top wall to the upper circle whole cavity for $Ra = 10^6$.

In case-III, the isotherm contours are parallel and closer to the adiabatic surface for $Ra = (10^3 - 10^5)$; And symmetrical twisted curves are closer to the adiabatic surface when the Rayleigh number becomes 10^6.

In case-IV, the parallel isotherm contours can be seen at the upper circular obstacle but circulation smooth contours are seen related to the lower circle for $Ra = (10^3 - 10^5)$. On the other hand, the symmetrical twisted isotherm contours are seen vertically inside the cavity. However, twisted smooth contours are noticed at the upper circle, and circulation contours are seen as related to the lower circle for $Ra = 10^6$.

In case-V, the isotherm contours are circulated parallel curves in the whole cavity for $Ra = (10^3 - 10^5)$ and twisted symmetric curves inside the cavity for $Ra = 10^6$.

Cases	$Ra = 10^3$	$Ra = 10^4$	$Ra = 10^5$	$Ra = 10^6$
Case-I	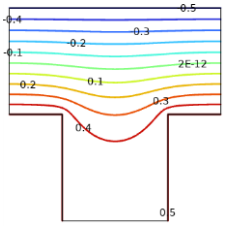	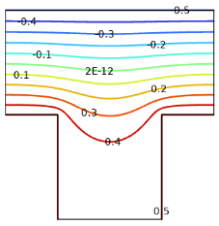	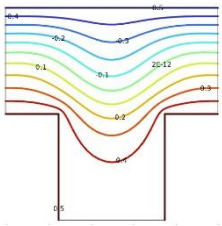	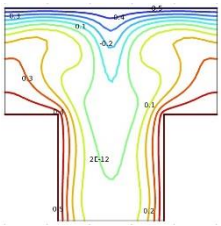

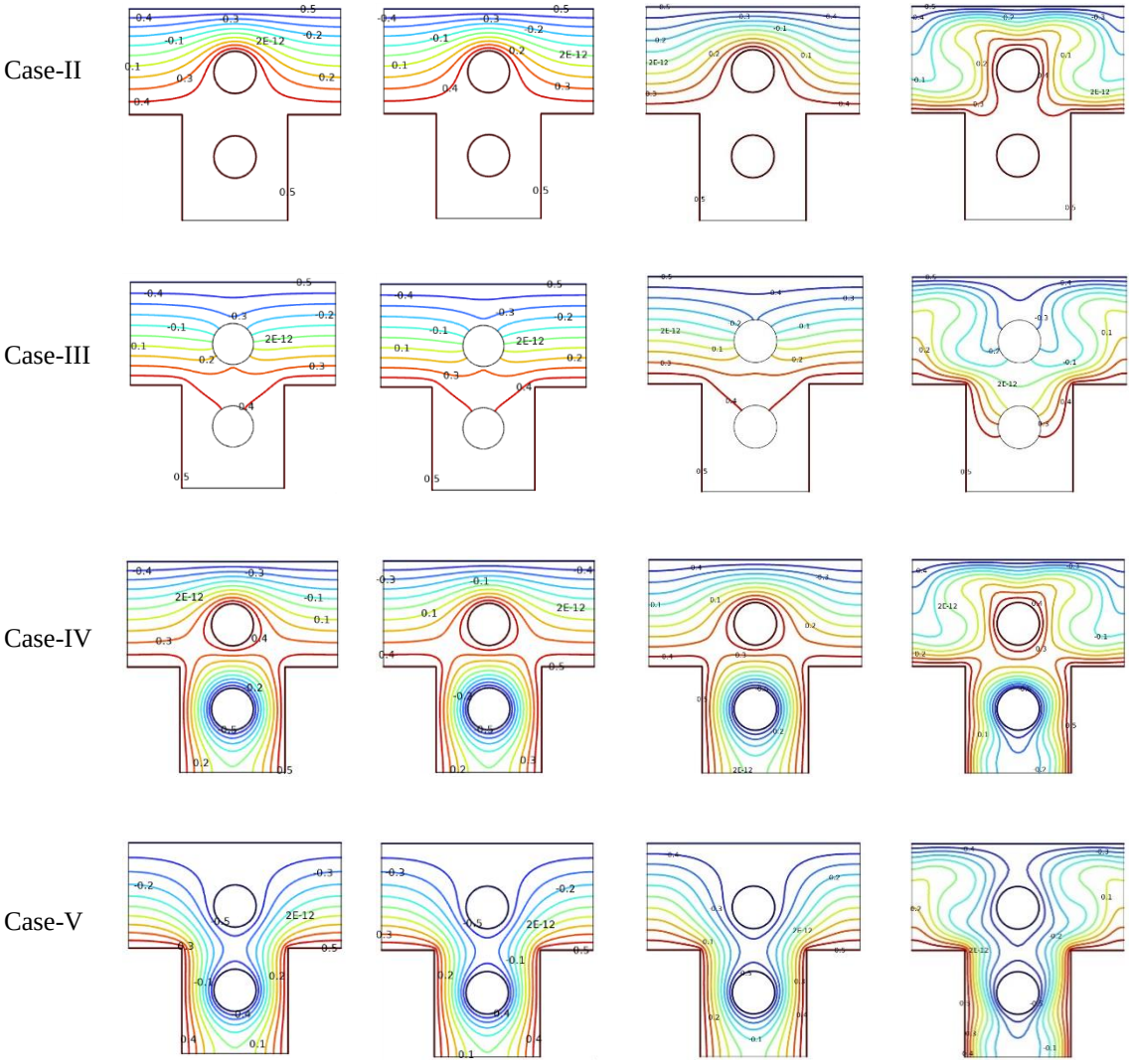

Fig. 5. Isotherm contours for varying Rayleigh Number ($Ra = 10^3 - 10^6$)

Average Nusselt-number

Here, the average Nusselt-number is calculated for varying Rayleigh numbers as shown in Table 2. It is shown in Figure 6 that with incorporating circular obstacles inside the enclosure thermal performance can be developed for increasing the Rayleigh numbers. However, after adding cool circular obstacles, the thermal performance of the enclosure can be improved highly for varying Rayleigh numbers.

Table 2 Average Nusselt-number Nu_{ave} for varying Ra

Cases	Ra=10^3	Ra=10^4	Ra=10^5	Ra=10^6
Case-I	1.7756	1.7756	1.9445	5.4967
Case-II	0.8347	0.8482	1.0724	3.1875
Case-III	1.6253	1.6252	1.6297	3.8871
Case-IV	5.2717	5.2889	5.5368	8.4320
Case-V	6.8648	6.865	6.9422	9.4967

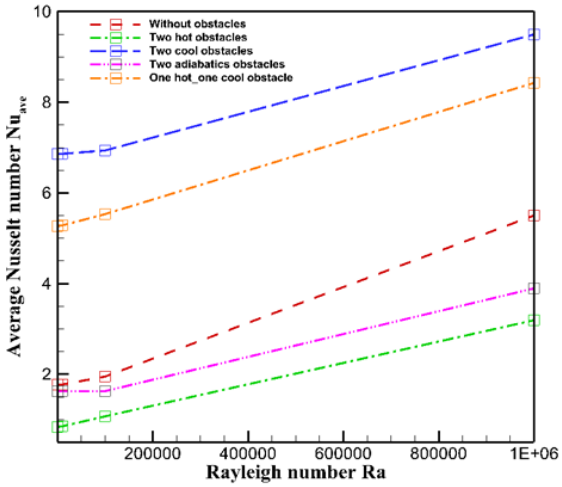

Fig. 6. Average Nusselt-number for five cases

Entropy Generation (E_{gen}) and Bejan Number (Be)

There can be considerable variations in the behavior of E_{gen} due to the temperature gradient, viscosity dissipation, total E_{gen}, and local Be contours at various thermal conditions of circular obstacles and without obstacles inside the T-shaped enclosure. Figure 7 shows the E_{gen} and local Be contours for five cases inside the cavity. Every contour can vary significantly at various Rayleigh numbers ($Ra = 10^5 - 10^6$). Convective factors dominate in forming fluid flow and determining E_{gen} at these elevated Ra levels. Consequently, the cases of a domain without cylinder and a domain with two circular cylinders exhibit observable differences in E_{gen}, highlighting the important influence of convection on the distribution of energy and entropy. In case-I, it is evident that a rise in Ra values cause the contours to significantly increase inside the whole cavity. At higher Ra, the contour shows a complex nature inside the enclosure without obstacles. After adding two circular obstacles with thermal boundary conditions, there is a significant change in entropy generation. In case-II and case-III, by analyzing the local entropy contours, we find that the graphs near the cold and adiabatic surface get denser with an increase in Ra. In case-IV and case-V, the contours of the isotherm reveal that when Ra rises, the contours around the heated and cold surface as well as the adiabatic surface get denser.

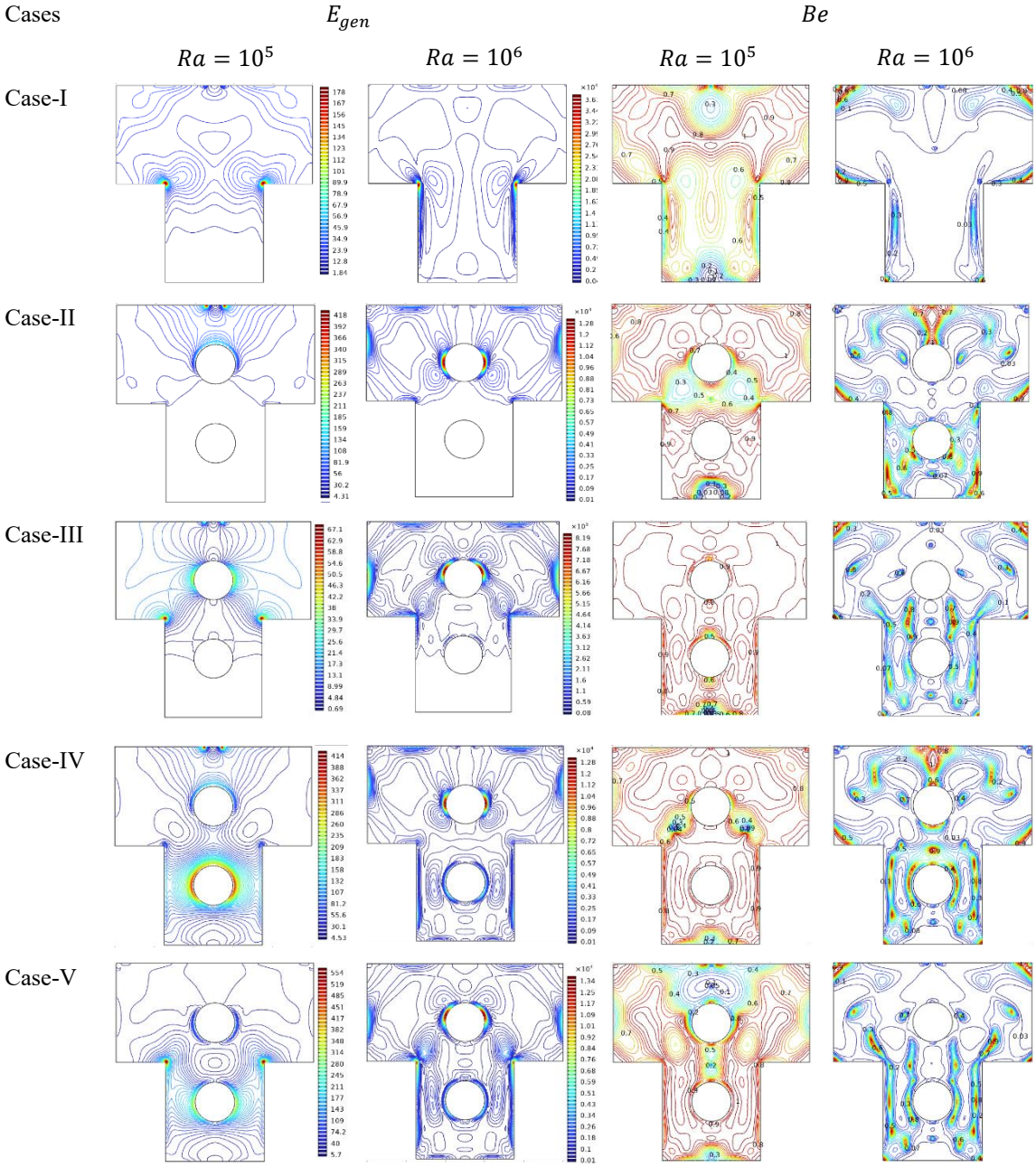

Fig. 7. Spatial Distribution of E_{gen} and Local Be for five cases at $Ra = 10^5 - 10^6$

When the Rayleigh number is increasing, the average E_{gen} is increasing which shows in Table 3. We get the best average entropy value in case-I and after including two obstacles the average entropy value is better in case-V than others as shown in Figure 8.

Table 3 Entropy Generation (E_{gen})

Case	Entropy Generation (E_{gen})			
	$Ra = 10^3$	$Ra = 10^4$	$Ra = 10^5$	$Ra = 10^6$
Case-I	1.8373	1.838	2.6712	155.85
Case-II	3.0397	3.0422	3.5379	79.405
Case-III	1.6834	1.6836	1.7308	70.11
Case-IV	8.3539	8.3597	9.1401	112.44
Case-V	7.0431	7.0535	8.4205	197.77

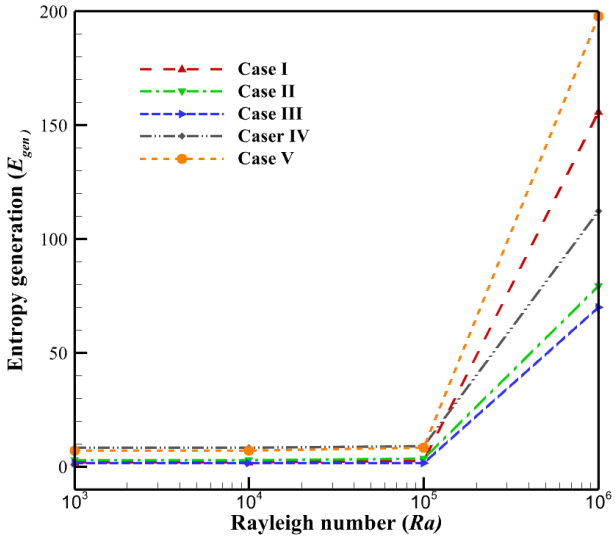

Fig. 8. Entropy generation for varying Rayleigh numbers

When E_{gen} is dominating due to heat transfer, it is seen that contours become less uniform as Ra increases, resulting in a significant fluctuation in temperature in the bottom region. Conversely, when the Rayleigh number is increasing, the local Bejan number (Be_l) is decreasing which shows in Table 4 and Figure 9. But when it comes to cavity flow analysis, a rise in Be means that the rate of heat transfer becomes more apparent than the rate of energy annihilation.

Table 4 Local Bejan Number (Be) for varying Rayleigh numbers

	Local Bejan Number (Be)			
Case	$Ra = 10^3$	$Ra = 10^4$	$Ra = 10^5$	$Ra = 10^6$
Case-I	0.99998	0.99762	0.72572	0.075872
Case-II	0.99959	0.99354	0.82371	0.18712
Case-III	1	0.99956	0.95674	0.23094
Case-IV	0.99999	0.99883	0.88297	0.13527
Case-V	0.99995	0.99517	0.74707	0.043229

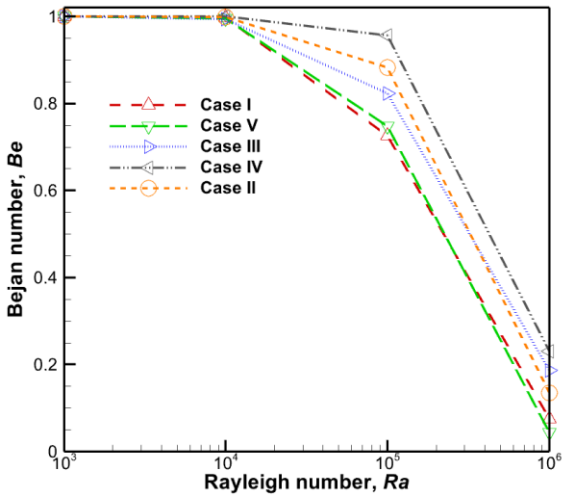

Fig. 9. Local Bejan Number (Be) for varying Rayleigh numbers

Ecological Coefficient performance ($ECOP = \frac{Nu_{ave}}{E_{gen}}$) [20] is affected by various Rayleigh numbers ($Ra = 10^3 - 10^6$). In case-I, at higher Ra, the $ECOP$ value is much lower than others which has a good effect on the environment.

Table 5 Ecological Coefficient Performance ($ECOP$) for varying Rayleigh numbers

	Ecological Coefficient Performance ($ECOP$)			
Case	$Ra = 10^3$	$Ra = 10^4$	$Ra = 10^5$	$Ra = 10^6$
Case-I	0.96642	0.9661	0.72795	0.03527
Case-II	0.27459	0.27881	0.30312	0.04014
Case-III	0.96549	0.96531	0.94159	0.05544
Case-IV	0.63105	0.63266	0.60577	0.07499
Case-V	0.97468	0.97328	0.82444	0.04801

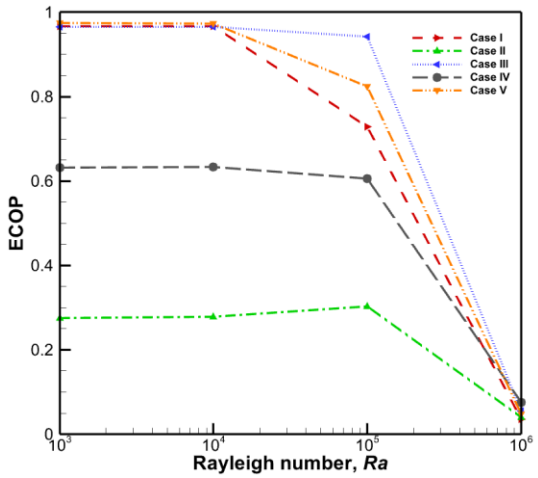

Fig. 10. $ECOP$ for varying Rayleigh numbers.

Suggesting that introducing obstacles into the domain improve thermal energy and minimize its impact on the environment. Additionally, Figure 10 shows that there is a decline in $ECOP$ values when Ra rises from 10^3 to 10^6, suggesting a lower level of energy efficiency and a greater environmental effect. Based on this pattern, it is possible that the lower ECOP values may be obtained from higher Ra values, which could mean a decrease in the system's energy efficiency and an increase in its environmental effect.

Conclusion

A numerical investigation of heat transfer and entropy generation on natural convection of airflow is performed inside the T-shaped cavity with and without circular obstacles. According to boundary conditions, five cases are considered in our flow simulation. Therefore, the highlighted conclusions are obtained as following:

(i) Streamlines and isotherm contours are depending on parameters such as the thermal conditions of obstacles and Rayleigh numbers.

(ii) When Rayleigh number increases, isotherm contours are spread smoothly and symmetrically inside the whole cavity.

(iii) Thermal performance can be controlled by adding circular obstacles inside the T-shaped cavity according to numerically calculated streamlines and thermal contours data.

(iv) For varying Rayleigh numbers, streamline contours are represented by symmetrical rotating vortices that can be observed in the entire cavity.

(v) The average Nusselt-number and entropy generation at the enclosure increase for increasing Rayleigh number.

(vi) The higher entropy value can be found in case-v than others cases.

(vii) Suggesting that introducing obstacles into the domain improve thermal energy and minimize its impact on the environment.

It is found that the thermal performance of the cavity can be improved by adding two circular obstacles (radius 0.05) at position (0.25, 0.1) and (0.25, -0.1) with cool boundary conditions. It is evident that the innovative structure by adding two circular obstacles with cool boundary conditions gives higher average Nusselt-number for varying Rayleigh numbers.

References

Alam MS, Billah MM, Hossain SMC, Keya SS and Haque MM. 2022. MHD influence on convective heat transfer in a semi-circular cavity using nonhomogeneous nanofluid model. Int. J. Thermofluids, 16: 100197.

Alhajaj Z, Bayomy AM, Saghir MZ and Rahman MM. 2020. Flow of nanofluid and hybrid fluid in porous channels: experimental and numerical approach. Int. J. Thermofluids, 1: 100016.

Alhashash A and Saleh H. 2023. Use of Finite Element Method for Free Convection of Nanofluids between a Rectangular Enclosure and a Sinusoidal Cylinder Using Buongiorno's Two-Phase Model. Advances in Mathematical Physics, 1–15. https://doi.org/10.1155/2023/8426825

Amahmid A, Hasnaoui M and Vasseur P. 1997. The multiplicity of solutions in natural convection under a repetitive geometry. Int. J. Heat and Mass Transfer 40(16): 3805–3818.

Asad MFA, Sarker MMA and Munshi MJH. 2019. Numerical investigation of natural convection flow in a hexagonal enclosure having vertical Fin. J. Sci. Res. 11 (2): 173–183.

Chaabane R, Kolsi L, Jemni A and D'Orazio A. 2022. Buoyancy driven flow characteristics inside a cavity equiped with diamond elliptic array. Inte. J. Nonlinear Sciences and Numerical Simulation, 24(6):2163–2177. https://doi.org/10.1515/ijnsns-2021-0073

Choi Stephen US. 1998. Nanofluid technology: current status and future research. Argonne National Lab. (ANL), Argonne IL, United States.

Das SK, Choi, Stephen US, Yu W and Pradeep T. 2007. Nanofluids: science and technology. John Wiley & Sons, Inc., Hoboken, New Jersey

Desrayaud G and Fichera A. 2002. Laminar natural convection in a vertical isothermal channel with symmetric surface-mounted rectangular ribs. Int. J. Heat and Fluid Flow, 23(4): 519-529.

El Alami M, Najam M, Semma E, Oubarra A and Penot F. 2004. Chimney effect in a "T" form cavity with heated isothermal blocks: The blocks height effect. Energy Conversion and Management, 45(20): 3181-3191.

Fayz-Al-Asad M, Munshi MJH, Bhowmik RK and Sarker MMA. 2019. MHD free convection heat transfer having vertical fin in a square wavy cavity. Int. J. Statist. Appl. Mathem., 4(3): 32-38.

Hossain MA, Podder C, and Saha BK. 2023. Effect on Natural Convection Heat Transfer in an Inclined Square Cavity with Uniformly and Non-Uniformly Heating side walls. Barishal University Journal of Science and Engineering, 8: 83-110.

Ilis GG, Mobedi M and Sunden B. 2008. Effect of aspect ratio on entropy generation in a rectangular cavity with differentially heated vertical walls. Int. Com. Heat and Mass Transfer, 35(6): 696-703.

Islam T, Akter N and Jahan N. 2020. MHD free convective heat transfer in a triangular enclosure filled with copper-water nanofluid. Int. J. Mat. Math. Sci, 2(2): 29-38.

Jani S, Amini M, and Mahmoodi M. 2011. Numerical study of free convection heat transfer in a square cavity with a fin attached to its cold wall. Heat Transfer Research, 42(3): 251-266.

Kuyper RA, Van Der Meer Th H, Hoogendoorn CJ,

and Henkes RAWM. 1993. Numerical study of laminar and turbulent natural convection in an inclined square cavity. Int. J. Heat and Mass Transfer, 36(11):2899–2911. https://doi.org/10.1016/0017-9310(93)90109-J

Kwak CE, and Song TH. 2000. Natural convection around horizontal downward-facing plate with rectangular grooves: experiments and numerical simulations. Int. J. heat and mass transfer, 43(5): 825-838.

Momoniat E, Harley C, and Herbst RS. 2023. Effects of extended surfaces on heat transfer in buoyancy-driven flow in a square cavity. Results in Engineering, 18:101190. https://doi.org/10.1016/j.rineng.2023.101190

Rahman MM, Alam MS, Al-Salti N and Eltayeb I A. 2016. Hydromagnetic natural convective heat transfer flow in an isosceles triangular cavity filled with nanofluid using two-component nonhomogeneous model. Int. J. Thermal Sciences, 107: 272-288.

Saboj JH, Nag P, Saha G and Saha SC. 2023. Entropy production analysis in an octagonal cavity with an inner cold cylinder: A thermodynamic aspect. Energies (Basel), 16 (14):5487. https://doi.org/10.3390/en16145487

Saghir MZ and Rahman MM. 2021. Brownian motion and thermophoretic effects of flow in channels using nanofluid: A two-phase model. Int. J. Thermofluids, 10:100085.

Saha BK, Jihan JI, Ahammad MZ, Saha G and Saha SC. 2024. Enhanced thermal performance and entropy generation analysis in a novel cavity design with circular cylinder. Heat Transfer, 53(3): 1446-1473. DOI: 10.1002/htj.22999.

Sheikholeslami M, Gorji-Bandpy M, Ganji DD and Soleimani S. 2014. Natural convection heat transfer in a cavity with sinusoidal wall filled with CuO–water nanofluid in presence of magnetic field. Journal of the Taiwan Institute of Chemical Engineers, 45(1): 40-49.

Shi X and Khodadadi JM. 2003. Laminar natural convection heat transfer in a differentially heated square cavity due to a thin fin on the hot wall. J. Heat Transfer, 125(4): 624-634.

Sreedevi P and Reddy PS. 2021. Entropy generation and heat transfer analysis of alumina and carbon nanotubes based hybrid nanofluid inside a cavity. Physica Scripta, 96(8): 085210.

Yousaf M and Usman S. 2015. Natural convection heat transfer in a square cavity with sinusoidal roughness elements. Int. J. Heat and Mass Transfer, 90: 180-190.